



Investigation of sedimentation, rheological, and damping force characteristics of carbonyl iron magnetorheological fluid with/without additives

M. N. Aruna¹ · M. R. Rahman¹ · Sharnappa Joladarashi² · Hemantha Kumar²

Received: 11 October 2019 / Accepted: 27 March 2020 / Published online: 11 April 2020
© The Brazilian Society of Mechanical Sciences and Engineering 2020

Abstract

In the present study, the magnetorheological fluid (MRF) samples are prepared using pure carbonyl iron particles (CIPs), CIPs/Claytone APA/Molyvan 855 additive, and friction reducer dispersed in poly-alpha-olefin oil. The scanning electron microscopy reveals that the Claytone additive morphology looks like a surface abundant in small folds, which connect the gaps between the spherical pure CIPs and prevent sedimentation in the MRF. The magnetic saturation properties are investigated through the vibrating sample magnetometer. The pure CIPs MRF shows (M_s) value as 146.12 emu/g, and the CIPs/Claytone APA/Molyvan indicates (M_s) as 55.12 emu/g. The magnetorheological flow curves, such as shear stress and viscosity as a function of shear rate, are investigated for the MRF samples through the magnetorheometer. The sedimentation analysis of the MRF is observed by visual inspection and shows that the CIPs/Claytone APA/Molyvan improved the sedimentation rate than the pure CIPs MRF. Finally, the experimental characterization of the prototype monotube MR damper is carried out using the hydraulic dynamic testing machine at 1.5 Hz frequency for damper peak–peak displacement length of ± 5 mm at three intervals of 0 h, 24 h, and 72 h in damper to know the effect on damping force for the prepared MRF samples against the sedimentation rate.

Keywords Carbonyl iron particles · Claytone APA · Sedimentation · Magnetorheology · Monotube MR damper · Magnetic saturation · Damping force · Poly-alpha-olefin oil

1 Introduction

In recent years, magnetorheological (MR) dampers are being widely investigated by researchers due to its superior features like fast response, low power consumption, and force controllability [1]. The magnetorheological fluids (MRF) suspensions generally consist of (20–40 vol%) micron-sized soft magnetic responsive particles dispersed in non-magnetic carrier fluids such as silicone, mineral,

synthetic oils, glycol, etc [2]. The first invention of MRF is credited to Rabinow [3]. In the absence of an external magnetic field (off-state) in the MRF, the particles are dispersed arbitrarily and act like Newtonian fluid [4]. When the MRF is subjected to the presence of an (on-state) external magnetic field, the dispersed magnetic particles get magnetized and build a column-like structure within the MRF, resulting in rheological flow properties such as off-state viscosity, yield stress, and elastic modulus [5, 6]. These controllable characteristics of MRF allow a series of applications like dampers, brakes, clutches, valves, and elastomeric mounts [7]. MR dampers are one of the promising new semi-active devices that contain MR fluid owing to change in its rheological properties when exposed to a magnetic field changing its damping force, which can be readily controlled within milliseconds and provide better ride comfort and stability than the active suspension systems [8]. For many applications of the MR damper, the most critical problem of the MRF is the sedimentation and caking [9]. A large density difference between a

Technical Editor: Edson José Soares, Ph.D.

✉ M. R. Rahman
rizwan@nitk.edu.in

¹ Department of Metallurgical and Materials Engineering, National Institute of Technology Karnataka, Surathkal, Mangalore, Karnataka 575025, India

² Department of Mechanical Engineering, National Institute of Technology Karnataka, Surathkal, Mangalore, Karnataka 575025, India

non-magnetic carrier medium and a dispersed magnetic phase causes the sedimentation problem [10]. The most commonly used magnetic particles in the MRF are still in use, i.e., carbonyl iron powder (CIPs) due to its soft magnetic properties, proper particle size availability, low magnetic hysteresis, and high magnetic permeability [11]. To avoid sedimentation problems in the MRF, several methods have been reported such as polymer coating materials like polystyrene [12], guar gum [13], polyaniline [14], and polymethacrylate [15] on magnetic CI particles, which are difficult and costly processes. As the polymer coating thickness increases on the outer surface of the particles, the MR effect decreases and reduces the dynamic yield stress during on-state rheology [16]. For this reason, the addition of additives to MRF suspensions is an effective method to reduce the sedimentation stability rate. Adding various submicron-sized additives such as fumed silica [17], graphene oxide [18], and carbon nanotubes [19] was found to enhance the sedimentation attracted to its high surface area and high aspect ratio. Additionally, it was found from the previous studies that clay additives such as attapulgite [20], sepiolite [21], organoclay [22], and halloysite [23] in the MRF considerably improved its dispersion stability. Based on MR damper force performance against settling of CIPs in the MRF, Liu et al. [24] reported that silica-coated MRFs improved its anti-corrosion properties and the damping force characteristics using the shear mode MR damper, which showed that the response time of CI particles was more than the coated MR fluid. Shah et al. [25] observed that plate-like iron particles showed low sedimentation in the MRF and verified this using small-sized MR damper for sedimentation test for 2 days. Most of the studies reported on MRF preparation

with less focus on MR damper performance against the settling of the MRF.

In present work, the effect on sedimentation stability, magnetic saturation, and magnetorheological properties of pure CIPs, CIPs/Claytone/Molyvan 855 additive, and friction reducer [26] MRF was examined. In addition, the MR damping performance was investigated and compared at three time intervals (0 h, 24 h, and 72 h) without disturbance of both the MRFs using a monotube MR damper.

2 Experimental

2.1 Materials used and chemical structures

Poly-alpha-olefin (PAO) oils are hydrogenated olefin oligomers/synthetic hydrocarbon, which is synthesized by catalytic polymerization of linear alpha-olefins. PAO fluid commonly called SpectraSyn poly-alpha-olefin fluid is purchased from ExxonMobil Chemical Co., as a base fluid. Synthesis involves mainly two steps: The first step is the synthesis of a mixture of oligomers that are polymers of relatively low molecular weight. Further, after the catalytic process, the second step of the manufacturing involves hydrogenation of unsaturated oligomers. The chemical structure is indicated in Fig. 1a, which is a very uniform comb-like structure [27]. Various properties such as high viscosity index, lower pour point, better thermal, and oxidation stability are superior when compared with mineral-based oils. The commercially available Molyvan 855 obtained is received from the Vanderbilt Chemicals, LLC, as a free sample for our research work. The Molyvan 855 is excellent oil-soluble molybdenum; each component works as a friction modifier/frictional

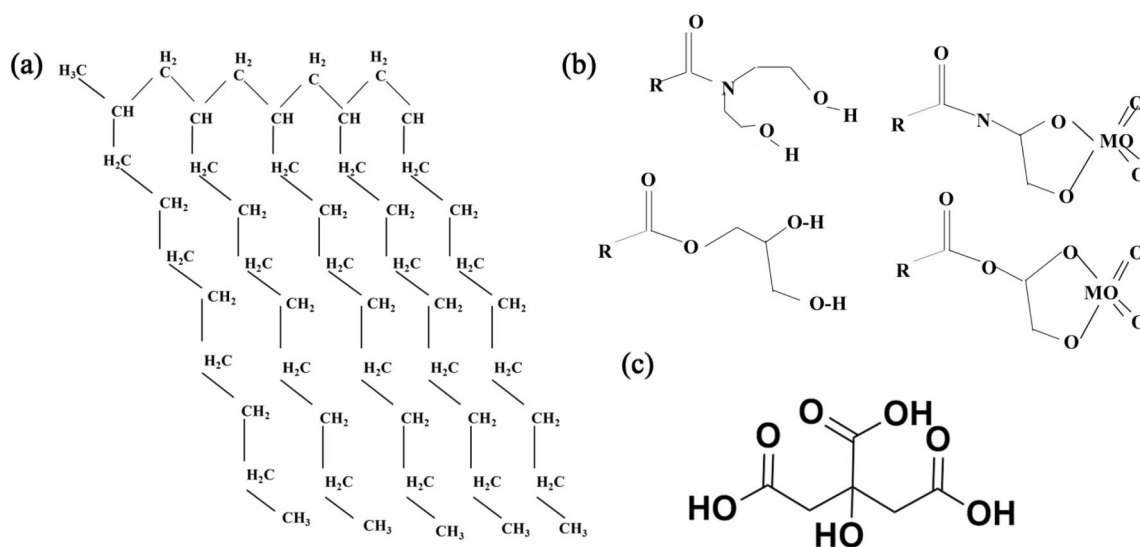


Fig. 1 Chemical structure of **a** poly-alpha-olefin oil (ExxonMobil Chemical Co.), **b** Molyvan 855 (R.T. Vanderbilt chemicals), **c** Claytone APA

reducer with better anti-wear and anti-oxidant properties that do not contain sulfur or phosphorus elements, used in lubricants [28, 29]. Figure 1b shows the chemical structure of Molyvan 855, having four components, and the MO group is responsible for the adequate friction-reducing agent. BYK Additives and Instruments provided the free sample of Claytone APA for our present work, and the chemical structure is shown in Fig. 1c. Claytone APA is a modified montmorillonite used as a rheology modifier additive generating excellent properties such as soft sediment and anti-settling agents. The recommended application of this clay is in paints, inks, and adhesives. Claytone APA is self-activating and readily dispersible for low to high polarity systems including alcohols, esters, and glycols [30].

2.2 MRFs preparation

Carbonyl iron particles (CIPs) with d50 average particle size ranging from 6 to 7 μm (CS grade) used as soft magnetic (99.5% Fe) dispersed phase particle were purchased from BASF Corp., and the poly-alpha-olefin (PAO) oil with a kinematic viscosity of $\nu = 17.2 \text{ mm}^2/\text{s}$ at 40 °C with a specific gravity (S. G=0.818) is the carrier medium for the MRFs. For preparing the MRFs, 70 wt% CIPs composition was added to both the samples. Moreover, 1 wt% Claytone APA was used

as an additive to improve the sedimentation in the MRFs and 1 wt% Molyvan 855 friction reducer agent. These MRF constituents were completely homogenized using a mechanical stirrer at 1000 rpm for 4 h. Table 1 shows the composition and samples of pure CIPs and CIPs/Claytone APA MRFs.

2.3 Fabrication of MR damper

Figure 2 shows a monotube MR damper of shear mode type without accumulator damper, which was fabricated to test against sedimentation of MRFs for low force applications. Figure 2a shows the schematic view of the proposed MR coil piston, and Fig. 2b indicates the 3D model view of the MR damper with copper coil winding, MRF, seals, housing cylinder, bearing, and piston rod. As the piston of the MR valve moves, the MRFs flow from the top to the bottom reservoir through the annular flow gap between the MR piston and the inner cylinder of the MR damper. Figure 3c shows the fabricated MR damper to know the damping performance of the prepared MRFs. To calculate the number of coils turns for the MR piston [31], Kirchhoff’s law was applied, which can be given by Eq. (1):

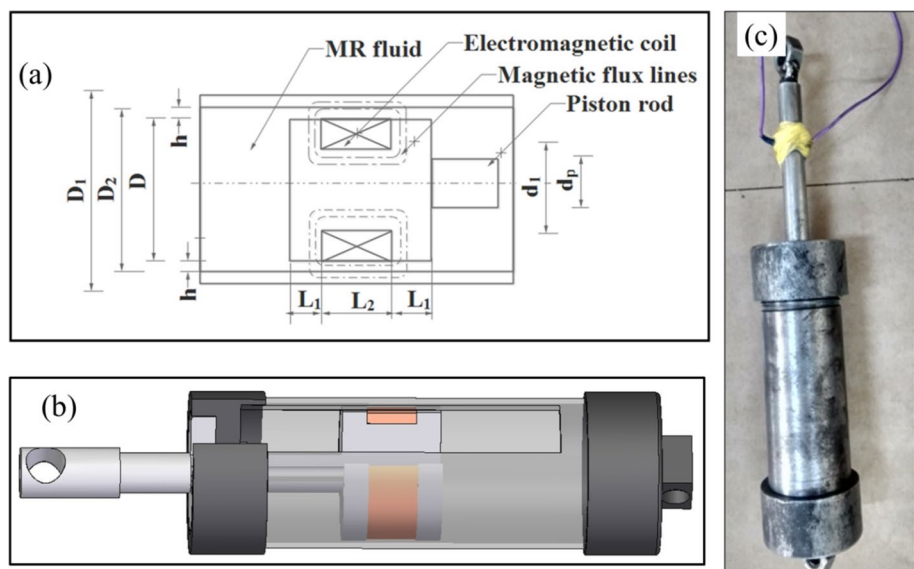
$$J = N_C I / A \tag{1}$$

where N_C is the number of coils turns in the electromagnetic coil, I is the applied current in DC, A is the area of the coil in m^2 , and J is the current density in A/m^2 . The number of turns was 278. All the dimensions and symbols of the MR damper are given in Table 1. Then, the approximate total damping force of the MR damper can be evaluated using the parallel-plate Bingham model, which is equal to the summation of the controllable F_r Eq. (3), frictional force F_f , and

Table 1 Composition and constituents used in MRFs

	CIPs (wt%)	PAO oil (wt%)	Claytone APA (wt%)	Molyvan 855 (wt%)
Pure CIPs MRF	70	30	None	None
CIPs/Claytone MRF	70	28	1	1

Fig. 2 Proposed MR damper **a** schematic drawing of MR piston, **b** 3D model view, and **c** fabricated MR damper



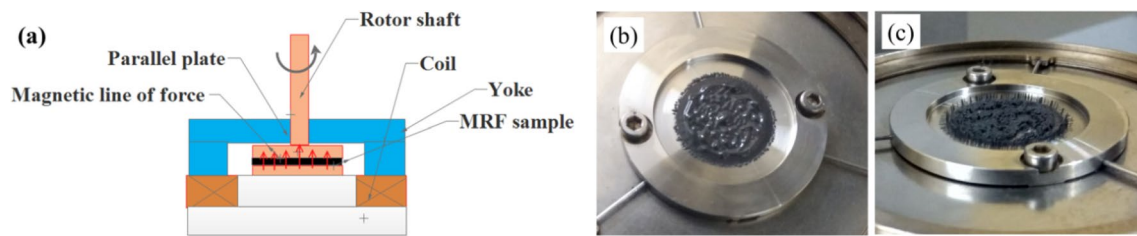


Fig. 3 **a** Magnetorheometer schematic, **b** MRFs sample without magnetic field strength ($H=0$), and **c** with the presence of magnetic field strength ($H>0$)

uncontrollable damping force Eq. (3). The total force in the MR damper F is given by Eq. (2) [32, 33]:

$$F = F_{\tau} + F_f + F_{\eta} \quad (2)$$

$$F_{\tau} = \left(2.07 + \frac{12Qn}{12Qn + 0.3w_0h^2\tau_0} \right) \left(\frac{\tau_0LA_p}{h} \text{sgn}(v_0) \right) \quad (3)$$

$$F_{\eta} = \left(1 + \frac{w_0hv_0}{2Q} \right) \left(\frac{12\eta QL_tA_p}{w_0h^3} \right) \quad (4)$$

The damping dynamic range D is given by Eq. (3):

$$D = \frac{F_{\tau}}{F_{uc}} = \frac{\text{Damper controllable force}}{\text{uncontrollably force} + \text{friction force}} = \frac{F_{\tau}}{F_{\eta} + F_f} \quad (5)$$

where h is the annular gap size, w_0 is the mean circumference of the damper, τ_0 is the field-dependent yield stress, η represents the viscosity of the MRF, v_0 is the piston head velocity, Q represents the volume flow rate $Q = A_p v_0$, L represents the effective axial pole length, and L_t is the total axial pole length.

2.4 Characterization

The morphology of the CIPs, raw Claytone APA, and CIPs/Claytone APA mixture was investigated via the scanning electron microscopy (SEM) (JEOL JSM-6380LA). The elemental composition of the pure CIPs was analyzed through the energy-dispersive spectroscopy (EDS). The magnetic saturation of CIPs in both types of MRF was measured using the vibrating sample magnetometer (VSM, Lakeshore, USA, Model 7407) at 300 K. The properties of the MRFs were measured using the twin drive magnetorheometer (MCR 701, TwinDrive Anton Paar, India) that produces magnetic field in the range of 0–255 kA/m integrated with an MRD cell-180 and a parallel-plate measuring system with a gap of 1 mm and diameter of 20 mm at 27 °C. The sedimentation ratio analysis of the CIPs and CIPs/Claytone APA-based MRFs was inspected visually. Figure 3 shows the physical

changes in the MRF sample in off-state and on-state, which were studied visually in the magnetorheometer. Figure 3a shows the schematic representation of the magnetorheometer, which consists of a rotor shaft, yoke, and the MRF sample. The MRF behaves like a normal fluid without magnetic field strength ($H=0$), as shown in Fig. 3b. With the application of magnetic field strength ($H>0$), the MRF appears like a robustly built column or shows fibril-like structures [34] as seen in Fig. 3c.

2.5 Damper test setup

The experimental setup of the dynamic testing machine (GEOTRAN) consists of a load cell, LVDT, DAQ, and signal generator, as indicated in Fig. 4a, and its schematic representation is shown in Fig. 4b. The frequencies, peak–peak displacement, and sedimentation testing of the MRF in the MR damper were set at 1.5 Hz of 5 mm at 0 h, 24 h, and 72 h. The applied current was changed from 0 to 0.4 A. The saturation of the applied current to the MR piston coil was limited to 0.4 A. Table 2 lists the MRF fluids tested for 0 h, 24 h, and 72 h without disturbing the incorporated MRF in MR damper (Table 3).

3 Results and discussion

3.1 SEM and EDS analysis

Figure 5a represents the morphology of the CIPs, which possess smooth surfaces and are spherical in shape. The energy-dispersive spectroscopy of the pure CIPs shows that it has Fe (99.02%) and O (0.11 wt%) with strong intensities. Figure 4b confirms that the CIPs are soft magnetic. Figure 5c shows the raw Claytone APA with an agglomerated structure with a surface abundant in folds. Figure 5d shows that the Claytone APA occupies the interspaces between the CIPs or is attached to the CIPs, which reduces the sedimentation rate of the Claytone APA-based MRFs [35].

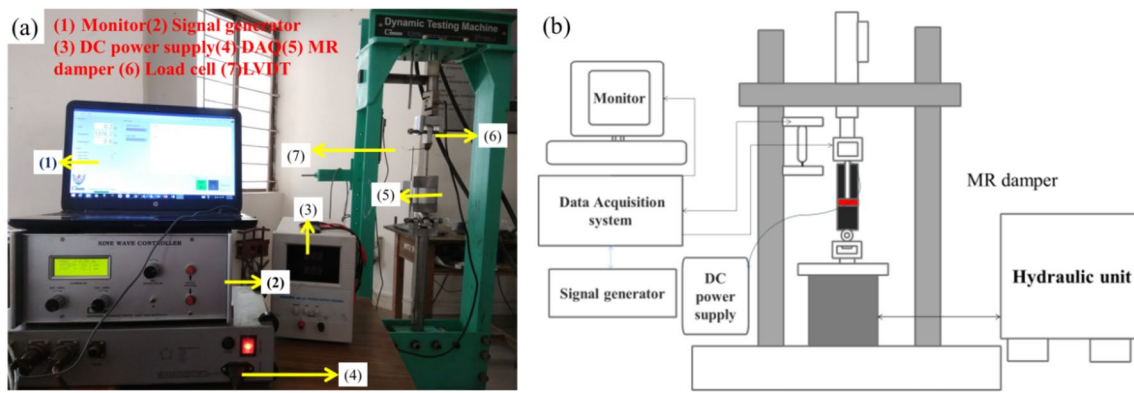


Fig. 4 a Experimental setup for MR damper and b schematic representation of the dynamic testing machine (DTM)

Table 2 Geometric dimensions of the MR damper

Parameters	Dimensions in mm
Outer cylinder diameter (D_1)	42
Inside cylinder diameter (D_2)	41
Length of the piston ($2L_1 + L_2$)	40
The diameter of the MR piston (D)	40
Length of the coil (L_2)	20
Annular flow channel gap (h)	1
The diameter of the piston rod (D_p)	12

3.2 VSM analysis

3.2.1 Measurement details

Using VSM, the magnetic saturation properties ($M-H$) curve is measured at room temperature with a standard commercially available liquid sample holder (i.e., No-730935 *Kel-F*[®]) from (Lakeshore, USA, Model 7407). Figure 6a, b shows a schematic representation of VSM measurements and dimensions of the liquid holder. The MR fluid is poured inside the holder in such a way by minimizing the small air bubbles and completely filling into the bottom cup to avoid the slushing of the liquid due to sample vibration. Then, the MRF sample is positioned with a plastic straw in the horizontal $X-Y$ and vertical Z -axis planes, and the sample is vibrated vertically about

the center point of the coil. The voltage is induced across the pickup coil, which is proportional to the magnetic moment of the MR fluid material [36].

3.2.2 Hysteresis curve analysis

Figure 7 shows the magnetization versus applied magnetic field (M vs. H) curve of the CIPs and CIPs/Claytone APA-based MRFs, which were measured using the vibrating sample magnetometer in the applied magnetic field varying from $-15,000$ to $15,000$ (Oe) at room temperature. The magnetic saturation (M_s) of the pure CIPs MRF was found to be 146.53 emu/g higher than that of CIPs/Claytone APA (55 emu/g). The M versus H curves indicate a big difference in saturation magnetization because the presence of Claytone APA additive will possess weak MR effect performance and reduce the saturation magnetization compared with pure CIPs-based MRF [37]. In case of additives added based on MRFs, 1 wt% of Claytone APA and 1 wt% Molyvan 855 additive are added while preparing MRFs suspension. On the other hand, these magnetic saturation differences are related to differences in the densities of magnetic CIPs in the samples. The density of CIPs in the liquid samples is smaller than that for the bare CIPs because they are dispersed in a liquid suspension. In other words, the actual mass of CIPs in the liquid samples is smaller than (CIPs + PAO + Claytone APA), so the calculated saturation magnetizations (emu/g) are reduced. Table 4 shows the properties of both the MRF samples by VSM analysis.

Table 3 MRF tested for 3 days without disturbing the MR damper

MRF type	Amplitude (Hz)	Displacement variation (mm)	Sedimentation (h)	Current (A)
CIPs MRF	1.5	0–5	0, 24 and 72	0 and 0.4
CIPs/Claytone MRF	1.5	0–5	0, 24 and 72	0 and 0.4

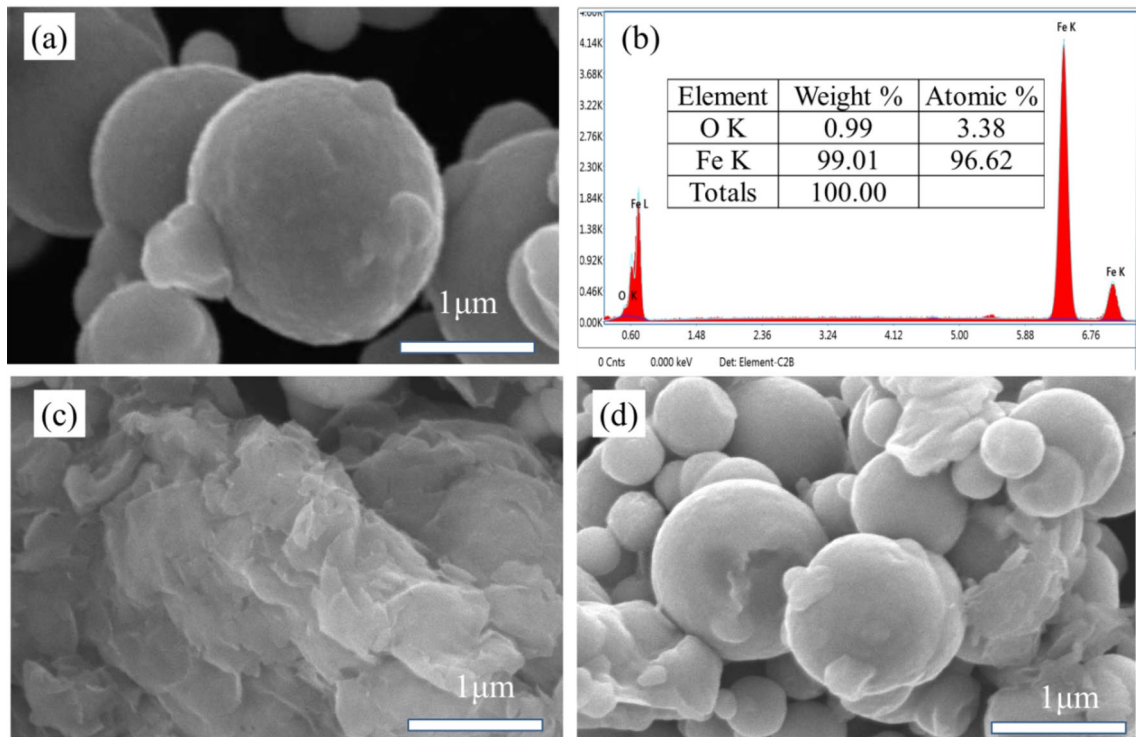
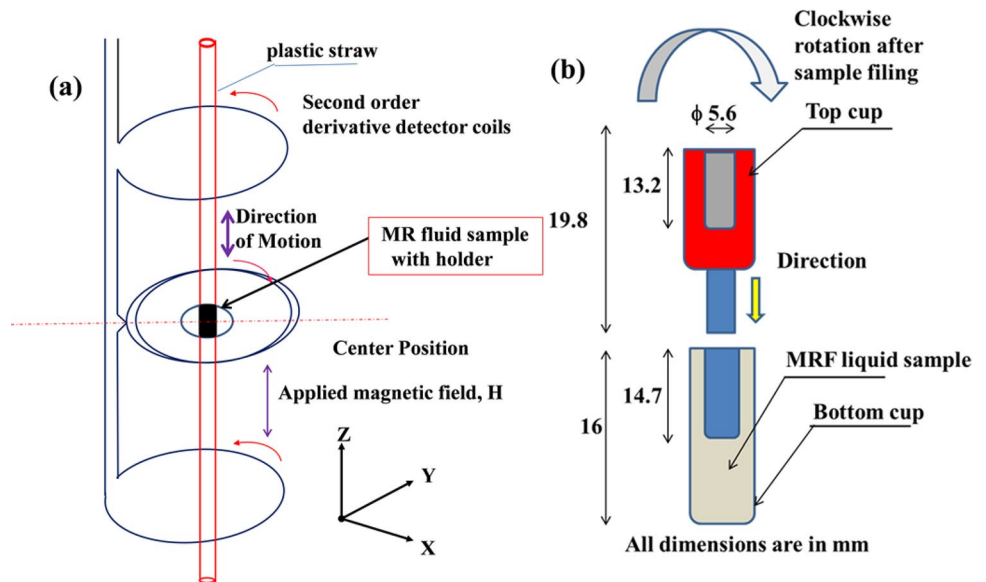


Fig. 5 SEM morphology of a pure CIPs, b EDS analysis, c pristine Claytone APA, and d CIPs/Claytone APA mixture

Fig. 6 a Schematic of representation of pickup coil geometry, b standard liquid sample holder for MRFs measurement type (730935 Kel-F) (figure based on the commercial instrument from Lak Shore Cryotronics)



3.3 Rheology analysis

Figure 8a represents shear stress versus shear rate ranging from 0.01 to 500 (1/s) on log–log scale for pure CIPs (closed symbols) and CIPs/Claytone APA (open symbols)-based MRFs subjected to different magnetic field strengths (0–255 kA/m) measured by a rotational twin drive MCR-701 rheometer. It was found that at zero

(0 kA/m) magnetic field strength, the shear stress of the CIPs and CIPs/Claytone APA MRFs exhibited a nonlinear relationship increasing the shear rate, which exhibits a typical non-Newtonian fluid behavior; it might be due to the high particle concentration and residual magnetization of CIPs [38, 39]. With increasing magnetic field strength, the shear stress of the pure CIPs and CIPs/Claytone APA MRF also increased. Figure 8a indicates that at

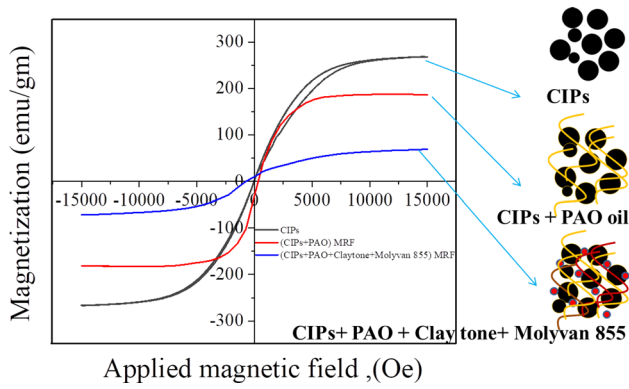


Fig. 7 Hysteresis loop from the VSM measurements a bare CIPs, CIPs + PAO oil, and CIPs + PAO + Claytone APA + Molyvan 855-based MRFs

Table 4 Magnetic properties of the prepared MR fluid samples

Parameters	CIPs-based MRF	CIPs/Claytone APA MRF
Coercivity (emu/g)	386.46	351.14
Magnetic saturation (emu/g)	146.12	55.24
Maximum field (Oe)	15,000	15,000
Retentivity (emu/g)	0.10795	0.001417

(255 kA/m) magnetic field strength, the shear stress values were about 15,100 Pa and 10,200 Pa for pure CIPs and CIPs/Claytone APA MRF samples at a maximum shear rate of 500 (1/s⁻¹), respectively. Both the MRF samples represented typical Bingham plastic model fluid behavior when the magnetic field strength was applied as given by Eq. (6). This is due to the formation of a robust column particle structure because of the dipole–dipole interaction

between the adjacent magnetic particles under the application of the magnetic field [40]:

$$\tau = \tau_y + \eta_p \dot{\gamma}, \quad \tau \geq \tau_y, \quad \dot{\gamma} = 0, \quad \tau \leq \tau_y, \quad (6)$$

where τ_y represents the dynamic yield stress $\dot{\gamma}$ given by shear rate, τ represents the shear stress, and η_p is the plastic viscosity.

Figure 8b clearly shows that the viscosity of the pure CIP MRFs is slightly lower than that of the CI/Claytone APA MRF at zero magnetic field strength. The viscosity decreases due to the change in the internal structure under shear deformation. It is due to the shear-thinning behavior effect for both the MRF samples. When the magnetic field is further increased, the free rotation of the magnetic particles is restricted, which increases the shear viscosity of the MRF samples to form a robust chain-like structure [41].

The relationship between the field-dependent dynamic yield stress and the strength of the magnetic field was fitted by the third-order polynomial equation and is depicted in Fig. 9a. A polynomial equation is extracted from this graph to evaluate the yield stress for any arbitrary value of magnetic flux strength between 0 and 255 kA/m. Equation (7) is obtained from the least square curve fitting method, wherein the third-order model provided accurate values with the adj- R^2 values fit method [42, 43]. Particularly at zero magnetic field strength, the yield stress values are positive values and are observed in Table 5

$$\tau_y = a + bH + cH^2 + dH^3 \quad (7)$$

where τ_y is the field-dependent yield stress (Pa), H is the magnetic field strength in kA/m, and a , b , c , and d are the fit constants.

A time-dependent field-induced shear stress measurement was performed for pure CIPs and CIPs/Claytone APA MRF as shown in Fig. 9b: Region I for off-state,

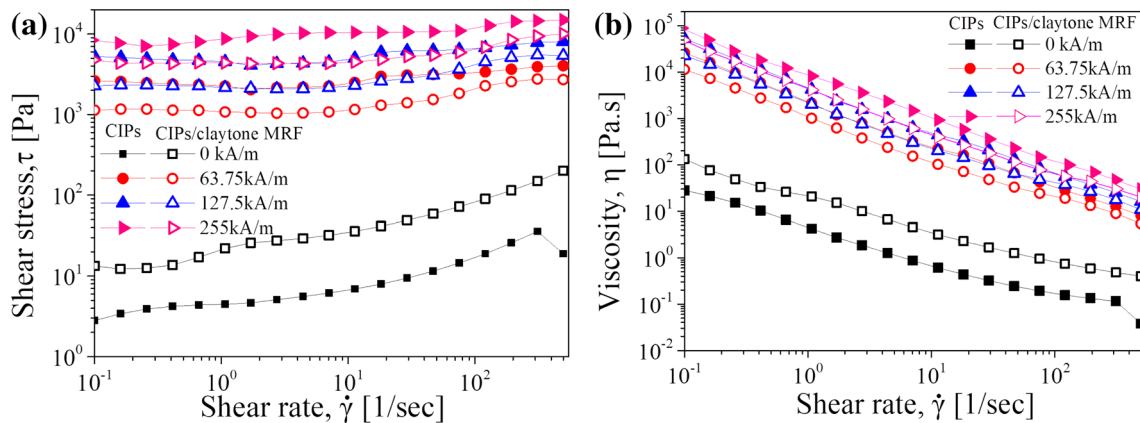


Fig. 8 a Shear stress versus shear rate and b viscosity versus shear rate for pure CIPs (closed symbols) and CIPs/Claytone APA (open symbols)-based MRFs under various magnetic field strengths

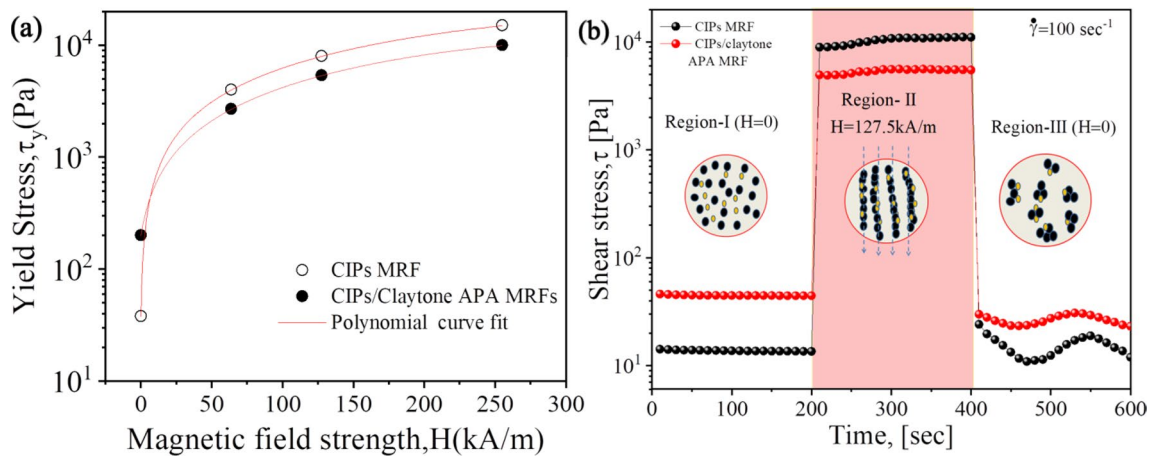


Fig. 9 **a** Dynamic yield stress (τ_y) as a function of magnetic field strength (H), and **b** shear stress versus time at a constant shear rate $\dot{\gamma} = 100 \text{ s}^{-1}$. The MRF of shear stress versus time measures in three

different regions. Region I: off-state, $H=0$ up to 0–200 s, Region II: on-state $H = 127.5 \text{ kA/m}$ from 200 to 400 s, and Region III: off-state $H=0$ from 400 to 600 s

Table 5 Optimal parameters of CIPs and CIPs/Claytone APA MRF-based suspensions by polynomial fitting

Sample name	<i>a</i>	<i>b</i>	<i>c</i>	<i>d</i>	Adj- <i>R</i> ²
CIPs MRF	37.388	60.128	0.03793	-1.74162×10^{-4}	0.99
CIPs/Clay- tone APA MRF	199.108	35.48	0.06656	-2.19589×10^{-4}	0.99

Region II for on-state, and Region III for off-state. From interval-I/Region I, it can be clearly observed that the magnetic field is in off-state condition, and the exhibited value of the pure CIPs MRF shear stress was found lower than that of CIPs/Claytone APA MRF. In Region II, the magnetic field present is on-state condition, i.e., 127.5 kA/m, and the value of the pure CIPs shear stress was higher than that of CIPs/Claytone APA MRFs, and also the shear stress increases rapidly due to the polarization force of the dipole–dipole interaction of the magnetic particles, which build robust column structures for both the MRFs. It can be seen from the Region III after the magnetic field is removed in the interval range of 400–600 s since the time scale of data acquisition is much faster than relaxation time after magnetic field is turned off; we observe an immediate decline in shear stress curve of CIPs MRFs, quite high sinusoidal in nature than the CIPs/Claytone APA MRFs. The decrease in shear stress with time is thought to be related to the effect of remanent magnetization ability to retain some amount of magnetization when the magnetic field is at the off condition. In contrast, column structures formed have not been broken, or the new aggregates have been re-arranged, which indicates the presence of large CIPs in the MR fluid. Similar observations have been reported by other workers [44–48].

This phenomenon also demonstrates in the inset figure the reversible transformation of microstructure formation of MRFs at off/on/off regions.

3.4 Sedimentation analysis

Figure 10a shows the sedimentation rate property of the two types of MR fluids inspected visually. Both the prepared MRFs were poured into a 10-ml cylinder, as seen in Fig. 10b, which shows the complete settlement of the MRFs in 7 days. The CIPs MRF settled down rapidly during the initial period and finally reached a stable value of 60.5%. Subsequently, the sedimentation ratio of the CI/Claytone APA MRF became slow due to the presence of additives and the friction reducer, which in turn slowed down the settling velocity of the CIPs, and the sedimentation ratio gradually reached a stable value at 82%. On the other hand, the CI/Claytone APA MRF demonstrated better sedimentation ratio than the pure CIPs MRF until 168 h. To find the sedimentation ratio, the equation commonly applied for MRFs is given by Eq. (8) [49]:

$$R\% = (A/A + B) * 100 \tag{8}$$

where *R* represents the sedimentation ratio, *b* is the height of the sedimentation MRF, and (*A* + *B*) represents the total height of the MRF.

3.5 MR damper performance of CIPs filled MRF

Figure 11 shows the damping force phenomenon of the CIPs-filled MRF for the first time with a peak–peak displacement of 5 mm and a frequency of 1.5 Hz. Figure 11a indicates that on the first day, the MR damper performance showed

Fig. 10 **a** Sedimentation versus time in hours and **b** MRF poured after complete settling of pure CIPs and CIPs/Claytone APA/friction reducer MRF in 7 days

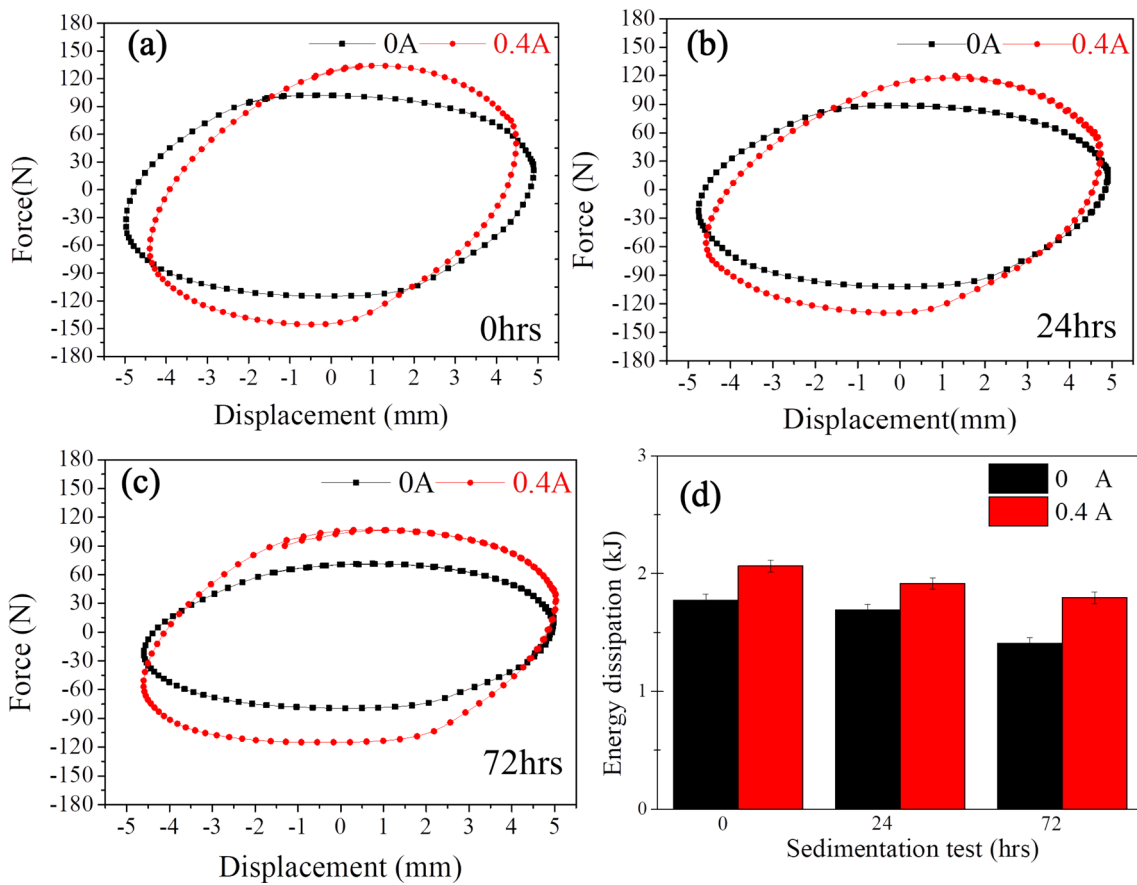
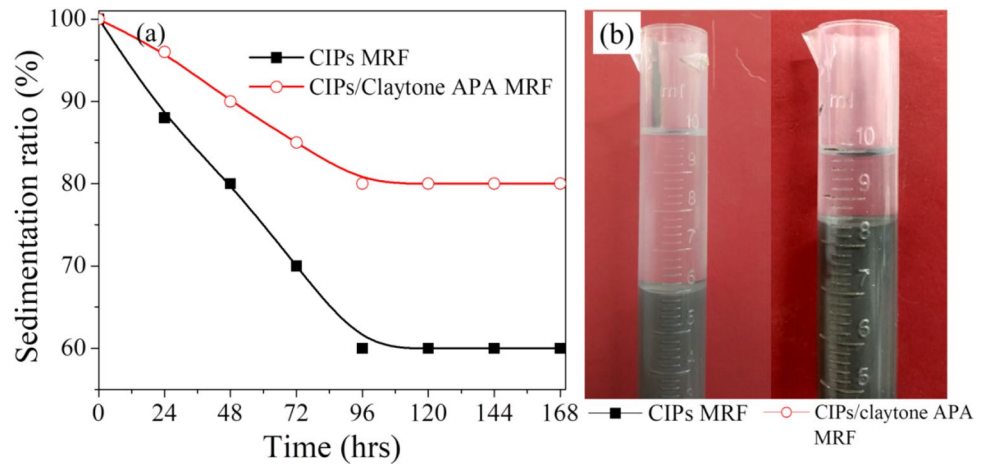


Fig. 11 Experimental damping force versus displacement loop characteristics of the MR damper operated vertically after incorporating the CIPs MRF against sedimentation days **a** 0, **b** 24, **c** 72 h, and **d** energy dissipation for 0 and 0.4 A at different sedimentation test days

off-state conditions, and the rebound and compression phase values of the damping force properties were +104.48 N and -114.16 N, respectively. At on-state conditions at 0.4 A, the rebound and compression damping forces increased to +133.64 N and -144.59 N, respectively. Figure 11b shows that after 24 h, the CIPs MRF sedimentation in the

MR damper performance showed off-state (the absence of magnetic field $I=0$ A) conditions, and the rebound and compression values of the damping force were +89.37 N and -102.12 N, respectively. At on-state (the presence of magnetic field $I=0.4$ A) condition, the rebound and compression damping forces increased to +117.59 N and -132.34 N,

respectively. From Fig. 11c, it was found that after 72 h, the CIPs MRF sedimentation in the MR damper performance showed off-state conditions, and the rebound and compression damping force values were +72.25 N and -87.92 N, respectively. At on-state condition of 0.4 A, the rebound and compression damping forces increased to +107.43 N and -111.18 N, respectively. These results suggest that variation in damping force, as listed in Table 6, is quite higher than the reported values when the applied current increases from 0 to 0.4 A [50].

It should be noted that the rebound and compression damping force reduces largely as the number of sedimentation days increases in the CIPs-filled MRF. The energy dissipation (E_d) values can be calculated using the area enclosed under force versus displacement each curve and dissipate more energy as applied current increases [51], as shown in Fig. 11d, and equivalent damping coefficient (C_e) is given by Eqs. (9) and (10) [52]. In addition, the energy dissipation decreases as the time period of the MRFs in the damper increases due to the effect of the gravitational settling of the CIPs in the MRFs:

$$E_d = \int f(t)du \quad (9)$$

$$C_e = \frac{E_d}{\pi f A^2} \quad (10)$$

where A represents the amplitude in m, f is the frequency (Hz), and F is the damping force (N).

3.6 MR damper performance of CIPs/Claytone APA-filled MRF

Figure 12 shows the damping force phenomenon of the displacement loop behavior properties of the CIPs/Claytone APA MRF for the first time by filling in a damper with peak-peak displacement amplitude of 5 mm and frequency of 1.5 Hz. Figure 12a indicates that on the first day, the MRF damper performance showed off-state conditions (0 A), and the rebound and compression damping force values were +97.22 N and -134.76 N, respectively. At an on-state conditions (0.4 A), the rebound and compression phase damping

forces increased to +116.88 N and -144.59 N, respectively. Figure 12b shows that after 24 h, the MRF sedimentation in the MR damper performance showed off-state conditions, and the rebound and compression values of the damping force were +94.21 N and -99.26 N, respectively. At on-state condition of 0.4 A, the rebound and compression damping forces increased to +108.55 N and -115.12 N, respectively. Figure 12c indicates that after 72 h, the MRF sedimentation in the MR damper performance showed off-state conditions, and the rebound and compression values of the damping force were +80.57 N and -82.61 N, respectively. At on-state condition of 0.4 A, the rebound and compression damping forces increased to +88.90 N and -94.74 N, respectively. Figure 12d indicates that the energy dissipation bar graph can be calculated using Eqs. (7) and (8). The CIPs/Claytone APA-based MRF in the damper energy dissipates less damping force, slightly lower as the number of sedimentation days increases than the CIPs-based MRF damper. Table 7 indicates that the damping force of rebound and the compression strokes of the CIPs/Claytone APA MRF-based damper at different sedimentation against time intervals is higher than the reported values [53].

4 Conclusions

In summary, the base magnetic CIPs with 70 wt% of solid loading along with plain PAO oil and CIPs/Claytone APA/Molyvan 855 as an additive, friction reducer was adjusted in PAO oil-based MRF was prepared to prevent the sedimentation problems. The dynamic yield stress and the shear stress of the CIPs/Claytone APA MRF were lower than those of the CIPs MRF. In addition, SEM confirmed that the surface of the CIPs connected well with Claytone APA, confirming improved sedimentation. The magnetic properties of the CIPs MRF showed higher saturation magnetization compared with the CIP/Claytone APA MRF. The fabricated MR damper against 72-h sedimentation testing of CIPs/Claytone MRF produced higher compression (F_{co}) and rebound (F_{re}) damping force than those of pure CIPs MRF at off-state (i.e., 0 A) condition, and also slightly lower compression (F_{co}) and rebound (F_{re}) damping force than CIPs MRF at on-state (i.e., 0.4 A) condition.

Table 6 Damping characteristics of MR damper CIPs-based MRF for different settling times

Rebound damping force (0 A) F_{Re} (N)	Compression damping force (0 A) F_{Co} (N)	Rebound damping force (0.4 A) F_{Re} (N)	Compression damping force (0.4 A) F_{Co} (N)	Frequency range (Hz)	Sedimentation time (h)
104.48	114.16	133.64	144.39	1.5	0
89.37	102.12	117.59	132.34	1.5	24
72.25	77.92	107.43	111.18	1.5	72

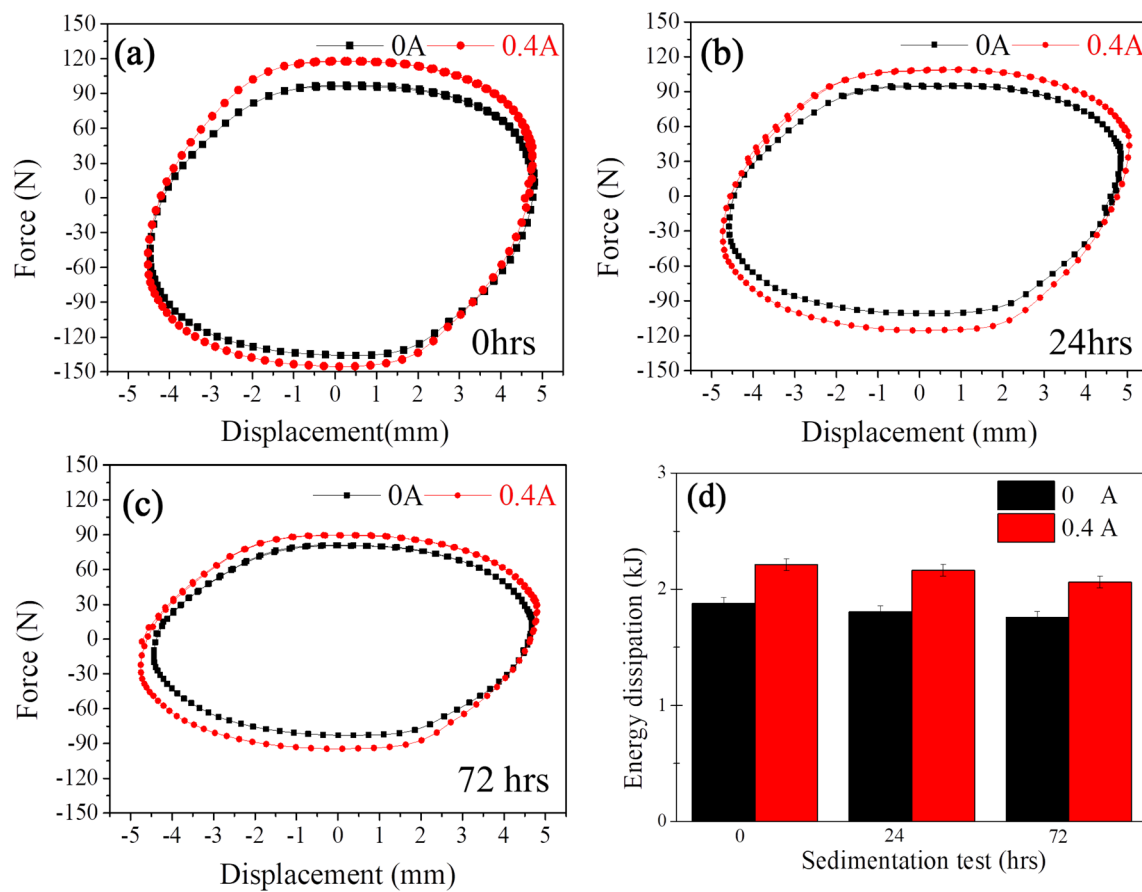


Fig. 12 Experimental damping force versus displacement loop characteristics of the MR damper operated vertically after incorporating the CIPs/Claytone APA MRF against sedimentation days **a** 0, **b** 24, **c** 72 h, and **d** energy dissipation for 0 and 0.4 A at different sedimentation test days

Table 7 Damping characteristics of MR damper CIPs/Claytone APA MRF-based MR fluids for different settling times

Rebound damping force (0 A) F_{Re} (N)	Compression damping force (0 A) F_{Co} (N)	Rebound Damping force (0.4 A) F_{Re} (N)	Compression Damping force (0.4 A) F_{Co} (N)	Frequency Range (Hz)	Sedimentation Time (h)
97.22	134.76	116.88	144.29	1.5	0
94.21	99.26	108.55	115.12	1.5	24
80.57	82.61	88.90	94.74	1.5	72

Acknowledgements This project was funded by IMPRINT India, Ministry of Human Resources Development, under the Government of India. The Project (No: 7330) is entitled “Development of Cost-Effective Magneto-Rheological (MR) Fluid Damper in Two Wheeler and Four Wheeler Automobiles to Improve Ride Comfort and Stability.”

References

- Dyke SJ, Spencer BF, Sain MK, Carlson JD (1996) Modeling and control of magnetorheological dampers for seismic response reduction. *Smart Mater Struct* 5:565–575. <https://doi.org/10.1088/0964-1726/5/5/006>
- Carlson JD (2008) Magnetorheological fluids. *Smart Mater* 252:17-1–17-8
- Rabinow J (1948) The magnetic fluid clutch. *Trans Am Inst Electr Eng* 67:1308–1315. <https://doi.org/10.1109/T-AIEE.1948.5059821>
- Yang Y, Li L, Chen G (2009) Static yield stress of ferrofluid-based magnetorheological fluids. *Rheol Acta* 48:457–466. <https://doi.org/10.1007/s00397-009-0346-z>
- De Vicente J, Klingenberg DJ, Hidalgo-Alvarez R (2011) Magnetorheological fluids: a review. *Soft Matter* 7:3701–3710. <https://doi.org/10.1039/c0sm01221a>
- Olabi AG, Grunwald A (2007) Design and application of magneto-rheological fluid. *Mater Des* 28:2658–2664. <https://doi.org/10.1016/j.matdes.2006.10.009>

7. Carlson JD, Catanzarite DM (1995) Commercial magneto-rheological fluid devices. In: 5th International conference on electro-rheological, magneto-rheological suspensions and associated technology, Sheffield, pp 10–14
8. Wang DH, Liao WH (2011) Magnetorheological fluid dampers: a review of parametric modelling. *Smart Mater Struct* 20:023001. <https://doi.org/10.1088/0964-1726/20/2/023001>
9. Park JH, Chin BD, Park OO (2001) Rheological properties and stabilization of magnetorheological fluids in a water-in-oil emulsion. *J Colloid Interface Sci* 240:349–354. <https://doi.org/10.1006/jcis.2001.7622>
10. Park BJ, Fang FF, Choi HJ (2010) Magnetorheology: materials and application. *Soft Matter* 6:5246–5253. <https://doi.org/10.1039/c0sm00014k>
11. Ashtiani M, Hashemabadi SH, Ghaffari A (2015) A review on the magnetorheological fluid preparation and stabilization. *J Magn Magn Mater* 374:711–715. <https://doi.org/10.1016/j.jmmm.2014.09.020>
12. Pu H-T, Jiang FJ, Yang ZL (2006) Preparation and properties of soft magnetic particles based on Fe₃O₄ and hollow polystyrene microsphere composite. *Mater Chem Phys* 100:10–14. <https://doi.org/10.1016/j.matchemphys.2005.11.032>
13. Wu WP, Zhao BY, Wu Q et al (2006) The strengthening effect of guar gum on the yield stress of magnetorheological fluid. *Smart Mater Struct* 15:N94. <https://doi.org/10.1088/0964-1726/15/4/N04>
14. Piao SH, Bhaumik M, Maity A, Choi HJ (2015) Polyaniline/Fe composite nanofiber added softmagnetic carbonyl iron microsphere suspension and its magnetorheology. *J Mater Chem C* 3:1861–1868. <https://doi.org/10.1039/c4tc02491e>
15. Kim MS, Cho MS, Choi HJ (2007) PMMA coated carbonyl iron microbeads and their magnetic characteristics. *Phys Status Solidi Appl Mater Sci* 204:4198–4201. <https://doi.org/10.1002/pssa.200777351>
16. Iglesias GR, López-López MT, Durán JDG et al (2012) Dynamic characterization of extremely bidisperse magnetorheological fluids. *J Colloid Interface Sci* 377:153–159. <https://doi.org/10.1016/j.jcis.2012.03.077>
17. Lim ST, Cho MS, Jang IB, Choi HJ (2004) Magnetorheological characterization of carbonyl iron based suspension stabilized by fumed silica. *J Magn Magn Mater* 282:170–173. <https://doi.org/10.1016/j.jmmm.2004.04.040>
18. Chen K, Zhang WL, Shan L et al (2014) Magnetorheology of suspensions based on graphene oxide coated or added carbonyl iron microspheres and sunflower oil. *J Appl Phys* 116:153508. <https://doi.org/10.1063/1.4898678>
19. Fang FF, Choi HJ, Jhon MS (2009) Magnetorheology of soft magnetic carbonyl iron suspension with single-walled carbon nanotube additive and its yield stress scaling function. *Colloids Surf A Physicochem Eng Asp* 351:46–51. <https://doi.org/10.1016/j.colsurfa.2009.09.032>
20. Chae HS, Piao SH, Maity A, Choi HJ (2014) Additive role of attapulgite nanoclay on carbonyl iron-based magnetorheological suspension. *Colloid Polym Sci* 293:89–95. <https://doi.org/10.1007/s00396-014-3389-3>
21. Piao SH, Zhang WL, Choi HJ (2014) Magnetic carbonyl iron suspension with sepiolite additive and its magnetorheological property. *IEEE Trans Magn* 50:1–4. <https://doi.org/10.1109/TMAG.2013.2278694>
22. Lim ST, Choi HJ, Jhon MS (2005) Magnetorheological characterization of carbonyl iron-organoclay suspensions. *IEEE Trans Magn* 41:3745–3747. <https://doi.org/10.1109/TMAG.2005.854759>
23. Hong CH, Liu YD, Choi HJ (2013) Carbonyl iron suspension with halloysite additive and its magnetorheology. *Appl Clay Sci* 80–81:366–371. <https://doi.org/10.1016/j.clay.2013.06.033>
24. Liu YD, Lee J, Choi SB, Choi HJ (2013) Silica-coated carbonyl iron microsphere based magnetorheological fluid and its damping force characteristics. *Smart Mater Struct* 22:065022. <https://doi.org/10.1088/0964-1726/22/6/065022>
25. Shah K, Phu DX, Seong MS et al (2014) A low sedimentation magnetorheological fluid based on plate-like iron particles, and verification using a damper test. *Smart Mater Struct* 23:027001. <https://doi.org/10.1088/0964-1726/23/2/027001>
26. Additives-organo NR, Baragel B, Rheological N, Cited R (2001) (12) United States Patent, 1
27. Emmett CJ, Hagemeyer MP, Harrington BA, Matsunaga PT, Nandapurkar PJ, Ruff CJ, Stavens KB (2016) U.S. Patent No. 9,399,746. U.S. Patent and Trademark Office, Washington, DC
28. Tanaka, N., Fukushima, A., Tatsumi, Y., & Saito, Y. (1997). U.S. Patent No. 5,627,146. Washington, DC: U.S. Patent and Trademark Office
29. Rowan EV, Farmer HH (1970) U.S. Patent No. 3,494,866. U.S. Patent and Trademark Office, Washington, DC
30. Zhang H, Zhou J, Muhammad Y, Tang R, Liu K, Zhu Y, Tong Z (2019) Citric acid modified bentonite for Congo Red adsorption. *Front Mater* 6:5. <https://doi.org/10.3389/fmats>
31. Nguyen QH, Choi SB (2009) Optimal design of a vehicle magnetorheological damper considering the damping force and dynamic range. *Smart Mater Struct* 18:015013. <https://doi.org/10.1088/0964-1726/18/1/015013>
32. Xu ZD, Jia DH, Zhang XC (2012) Performance tests and mathematical model considering magnetic saturation for magnetorheological damper. *J Intell Mater Syst Struct* 23:1331–1349. <https://doi.org/10.1177/1045389X12445629>
33. Gurubasavaraju TM, Kumar H, Arun M (2017) Evaluation of optimal parameters of MR fluids for damper application using particle swarm and response surface optimisation. *J Braz Soc Mech Sci Eng* 39:3683–3694. <https://doi.org/10.1007/s40430-017-0875-9>
34. Yu M, Ju B, Fu J et al (2014) Magnetoresistance characteristics of magnetorheological gel under a magnetic field. *Ind Eng Chem Res* 53:4704–4710. <https://doi.org/10.1021/ie4040237>
35. Aruna MN, Rahman MR, Joladarashi S, Kumar H (2019) Influence of additives on the synthesis of carbonyl iron suspension on rheological and sedimentation properties of magnetorheological (MR) fluids. *Mater Res Express* 6:086105. <https://doi.org/10.1088/2053-1591/ab1e03>
36. Boekelheide Z, Dennis CL (2016) Artifacts in magnetic measurements of fluid samples. *AIP Adv* 6(8):085201. <https://doi.org/10.1063/1.4960457>
37. Sidpara A, Das M, Jain VK (2009) Rheological characterization of magnetorheological finishing fluid. *Mater Manuf Process* 24:1467–1478. <https://doi.org/10.1080/10426910903367410>
38. Kim MW, Han WJ, Kim YH, Choi HJ (2016) Effect of a hard magnetic particle additive on rheological characteristics of microspherical carbonyl iron-based magnetorheological fluid. *Colloids Surf A Physicochem Eng Asp* 506:812–820. <https://doi.org/10.1016/j.colsurfa.2016.07.070>
39. Kim YH, Sim B, Choi HJ (2016) Fabrication of magnetite-coated attapulgite magnetic composite nanoparticles and their magnetorheology. *Colloids Surf A Physicochem Eng Asp* 507:103–109. <https://doi.org/10.1016/j.colsurfa.2016.07.095>
40. Kwon SH, Choi HJ, Lee JW et al (2013) Magnetorheology of xanthan-gum-coated soft magnetic carbonyl iron microspheres and their polishing characteristics. *J Korean Phys Soc* 62:2118–2122. <https://doi.org/10.3938/jkps.62.2118>
41. Bae DH, Choi HJ, Choi K et al (2017) Microcrystalline cellulose added carbonyl iron suspension and its magnetorheology. *Colloids Surf A Physicochem Eng Asp* 514:161–167. <https://doi.org/10.1016/j.colsurfa.2016.11.052>
42. Nguyen QH, Choi SB (2008) Optimal design of a vehicle magnetorheological damper considering the damping force and

- dynamic range. *Smart Mater Struct* 18(1):015013. <https://doi.org/10.1088/0964-1726/18/1/015013>
43. Tharehalli Mata G, Kumar H, Mahalingam A (2019) Performance analysis of a semi-active suspension system using coupled CFD-FEA based non-parametric modeling of low capacity shear mode monotube MR damper. *Proc Inst Mech Eng Part D J Automob Eng* 233:1214–1231. <https://doi.org/10.1177/0954407018765899>
44. Chand M, Kumar S, Shankar A et al (2013) The size induced effect on rheological properties of Co-ferrite based ferrofluid. *J Non Cryst Solids* 361:38–42. <https://doi.org/10.1016/j.jnoncrystol.2012.10.003>
45. Chand M, Shankar A, Jain K et al (2014) Improved properties of bidispersed magnetorheological fluids. *RSC Adv* 4:53960–53966. <https://doi.org/10.1039/c4ra07431a>
46. Yang P, Yu M, Fu J, Luo H (2018) Rheological properties of dimorphic magnetorheological gels mixed dendritic carbonyl iron powder. *J Intell Mater Syst Struct* 29(1):12–23. <https://doi.org/10.1177/1045389X17692050>
47. Wang G, Ma Y, Tong Y, Dong X (2016) Synthesis, characterization and magnetorheological study of 3-aminopropyltriethoxysilane-modified Fe_3O_4 nanoparticles. *Smart Mater Struct* 25(3):035028. <https://doi.org/10.1088/0964-1726/25/3/035028>
48. Arief I, Mukhopadhyay PK (2017) Yielding behavior and temperature-induced on-field oscillatory rheological studies in a novel MR suspension containing polymer-capped Fe_3Ni alloy microspheres. *J Magn Magn Mater* 429:236–240. <https://doi.org/10.1016/j.jmmm.2017.01.048>
49. Wang G, Ma Y, Li M et al (2017) Magnesium ferrite nanocrystal clusters for magnetorheological fluid with enhanced sedimentation stability. *Solid State Sci* 63:70–75. <https://doi.org/10.1016/j.solidstatesciences.2016.11.015>
50. Shah K, Xuan Phu D, Choi SB (2014) Rheological properties of bi-dispersed magnetorheological fluids based on plate-like iron particles with application to a small-sized damper. *J Appl Phys* 115:203907. <https://doi.org/10.1063/1.4879681>
51. Hemanth K, Kumar H, Gangadharan KV (2017) Vertical dynamic analysis of a quarter car suspension system with MR damper. *J Braz Soc Mech Sci Eng* 39:41–51. <https://doi.org/10.1007/s40430-015-0481-7>
52. Snyder RA, Kamath GM, Wereley NM (2001) Characterization and analysis of magnetorheological damper behavior under sinusoidal loading. *AIAA J* 39:1240–1253. <https://doi.org/10.2514/2.1466>
53. Kwon SH, Hong CH, Do PX et al (2015) Magnetorheology of a carbonyliron microsphere suspension with a halloysite additive and its damping force characteristics. *Ind Eng Chem Res* 54:4655–4663. <https://doi.org/10.1021/acs.iecr.5b00233>

Publisher's Note Springer Nature remains neutral with regard to jurisdictional claims in published maps and institutional affiliations.